Experimental and numerical analysis of compression behaviour of 3D printed metal foams

Journal of Physics: Conference Series **1706** (2020) 012213 doi:10.1088/1742-6596/1706/1/012213

Experimental and numerical analysis of compression behaviour of 3D printed metal foams

R Ramesh[1], **A S Prasanth**[2], **R Krishna**[1], **K KoushikSundaram**[1], **R Arul MozhiSelvan**[1] **and Abhishek Roy**[1]

[1]PSG Institute of Technology and Applied Research, Coimbatore - 641062, India
[2]PSG College of Technology, Coimbatore - 641004, India

Email: asp.mech@psgtech.ac.in

Abstract. This article focuses on comparing the experimental and numerical compressive behaviour of metal foams. The metal foams were initially modelled in three configurations of pore sizes. Each configuration was 3D printed using a laser sintering metal additive manufacturing technique. Subsequently, quasi-static compression tests were conducted and their stress-strain curves were examined to ascertain the proof stress of the three configurations. A numerical simulation of the compressive behaviours of the three foams was then conducted and their results were correlated with those from experimentation to quantify the error in simulation. The compression tests revealed that, the compressive strength was a function of density and porosity of the metal foams. Further, the numerical results of compression behaviours were validated, with less than 5 % deviation from the experimental results for all three foam configurations.

1. Introduction

Metal foams are engineered materials that possess numerous beneficial properties such as high energy absorptivity, low density, elevated stiffness and erosion resistance. These advantageous properties coupled with ease of manufacturing, facilitate widespread use of metal foams in multi-functional applications namely biomedical prosthesis, structural components in automotive and flight vehicles, lightweight panels and engineering functions involving impact resistance [1,2]. Traditionally, metal foams are manufactured by metallic melt or Powder Metallurgy (PM) routes. The PM route has limitations in producing metal foams with large volume fractions whereas metallic melt requires using specialized techniques such as blowing agents, injecting gas into the molten metal and maintaining stringent process conditions [3]. To overcome the constraints of legacy techniques, metal additive manufacturing, also referred to as metal 3D printing (3DP) is utilized to fabricate metal foams. 3DP techniques possess advantages of scalability, maintaining high dimensional accuracy and the ability to manufacture complex shapes [4]. Although numerous studies have elaborated on, the mechanical properties of foams manufactured employing traditional methods, a dearth of literature with focus on metal foams fabricated using 3DP techniques, exists. Therefore, in this study, compressive behaviour of 3D printed metal foams is analyzed through experimental and simulation methods. Further, a comparison of both the methods is performed to validate the numerical model with the measurements from compression stress-strain curves.

2. Materials and methods

The steps followed in modelling, 3D printing, compression testing and simulation are delineated in this section, hereunder.

2.1. Modeling of metal foams

The open cell metallic foams were initially modelled using Solidworks designing software. Three open cell foams of dimensions 1 inch cube (25.4 x 25.4 x 25.4 mm^3) were modelled. Each of the specimens comprised of three pore sizes of 3 mm, 2.5 mm and 2 mm as listed in table 1. The strut thickness of the foams was varied in the range of 0.7 mm to 1 mm to ensure structural stability and to avoid premature collapse of the foam during 3D printing. The porosities of the foams were determined using equation (1).

$$p = \frac{\rho_w - \rho_f}{\rho_w} \times 100 \quad (1)$$

where, ρ_w is the density of foam structure without pores and ρ_f represents the density of the porous foam. The specimens were then weighed to quantify their density as listed in table 1. A prototypical model of the foam is shown in figure 1.

Table 1. Specifications of metallic foams.

S.No	Designation	Poresize (mm)	Porosity (%)	Density (kg/m^3)
1	Specimen 1	3	71	2310
2	Specimen 2	2.5	67.87	2560
3	Specimen 3	2	72.51	2190

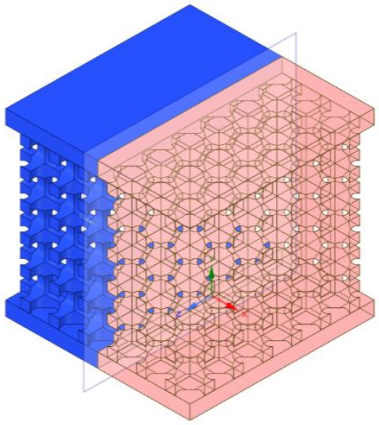

Figure 1. CAD model of metal foam.

2.2. Manufacturing of metal foams

Subsequent to modelling, the CAD models were converted to stereolithography (STL) format. The STL files were imported to a Fastform 3D printer capable of a build volume of 140 mm^3, each side. The three dimensionally identical specimens with varied pore sizes were 3D printed by laser sintering of AISI316L spherical prealloyed stainless steel powders. The specimens were simultaneously printed within nine hours and were not subjected to post-process heat treatment. As evident from table 1, the specifications reveal that, porosity and density vary with pore size of the three metallic foams.

2.3. Compressive test on metal foams

The compressive behaviour of the three specimens was assessed using a Zwick Roell Universal Testing Machine with a maximum rated load capacity of 100 kN. The uni-axial compression tests for the three specimens were performed up to a strain rate of 20 % in accordance with ASTM D695 standard and with a crosshead speed of 1.3 mm/min.

Table 2. Material Properties for simulation model.

S.No	Property	Unit	Value
1	Density	kg/m^3	7969
2	Young's Modulus	GPa	194.96
3	Thermal Conductivity	W/m^{o}C	14.21
4	Specific Heat	J/kg^{o}C	486.07
5	Yield Strength	MPa	229.6

2.4. Numerical simulation of metal foams

The CAD models of the three specimens were imported to the Transient structural module of ANSYS2020R1. The material properties of the AISI316L alloy utilized for numerical analysis of the three configurations are tabulated in table 2. Since the numerical models were subjected to plastic deformation, an adaptive, non-linear mesh of element size less than 1 mm was selected as depicted in figure 2. In order to boost the speed and performance of computation, the graphics processing unit (GPU) overide command is utilized. The GPU used for the present analysis is NVIDIA GeForce GTX 1050 Ti. The GPU utilizes a Pascal architecture with a clock speed of 1392 MHz, memory speed of 7 Gbps and a frame buffer of 4 GB GDDR5. Additionally, since the GPU comprises of 768 CUDA cores, it is best suited for mathematical calculations or solving complex mathematical models.

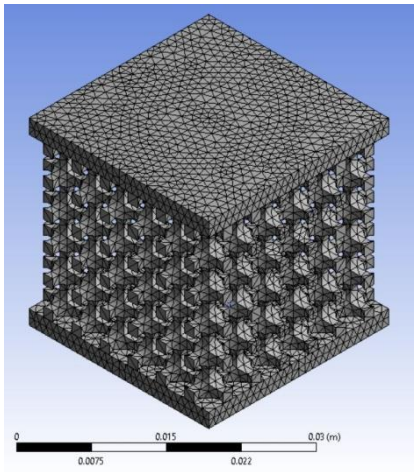

Figure 2. Meshed model for numerical analysis.

3. Results

As mentioned in sections 2.1 and 2.2, the open cell foams were modelled using CAD software and then 3D printed. Figure 3 shows the metal foams with three varying pore sizes of 3 mm, 2 mm and 2.5 mm. The three foams were then subjected to compressive loading as detailed in section 2.3. The

resulting stress-strain curves of the open cell foams with three different pore sizes are plotted in figure 4. The stress-strain plots indicate that, the mechanism of foam collapse follows the process of quasi-static failure followed by densification. When subjected to a compressive load, stress concentration occurs on the weakest strut in the most fragile layer of the entire foam structure. The failure of this strut cascades to a local failure of several layers, resulting in the collapse of the entire foam structure. Subsequent to local failure of the struts, densification occurs [5].

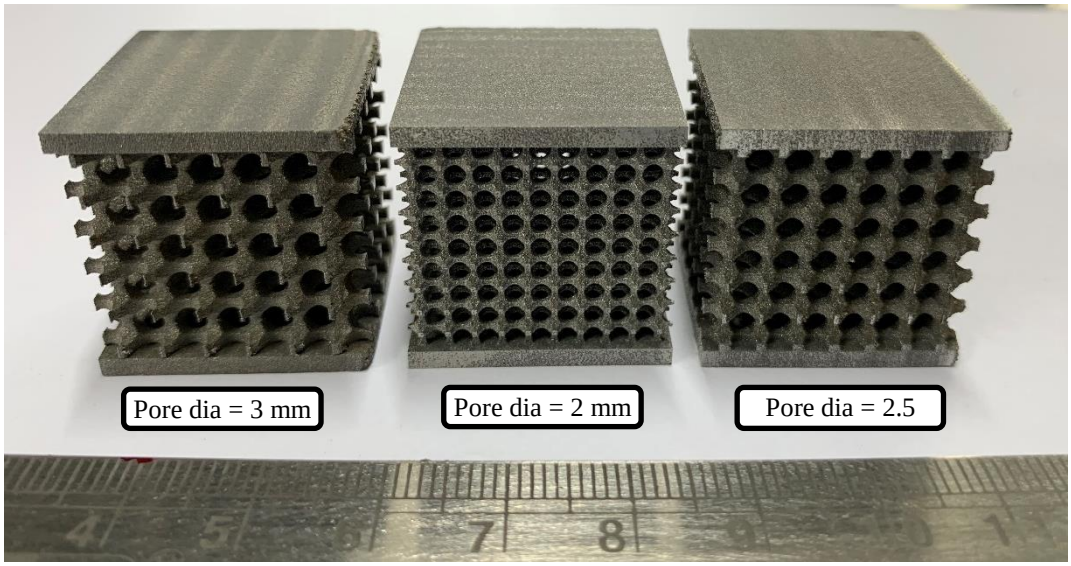

Figure 3. The 3D printed metal foams.

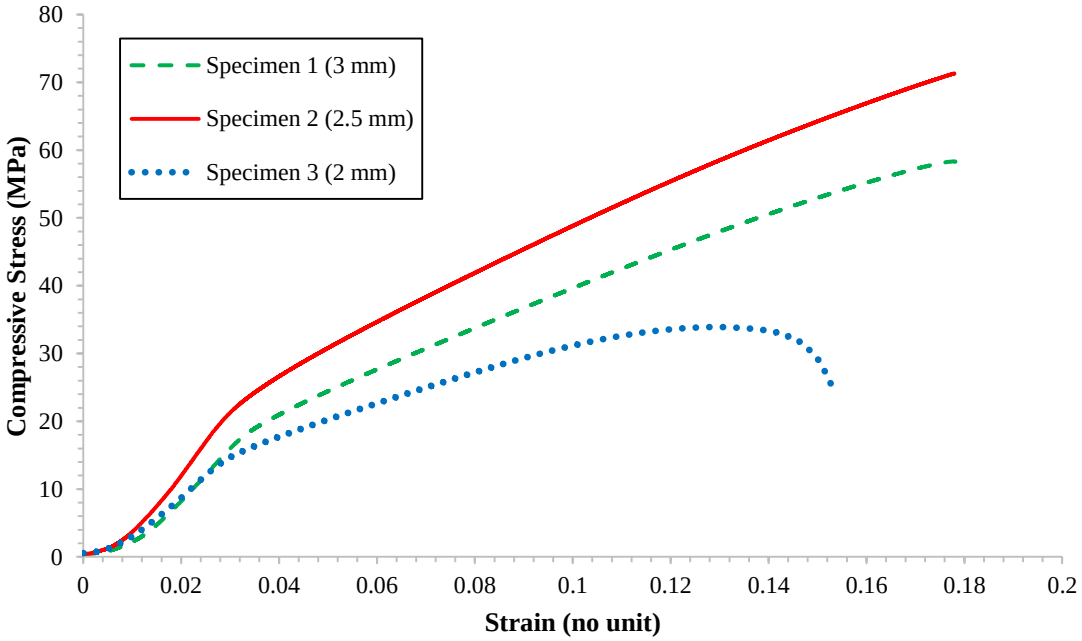

Figure 4. Compressive stress-strain behaviours of metal foams.

Densification follows a two-step approach. In step 1, the failed vertical struts, slip into the adjacent pores. As the applied load is further increased, these vertical struts begin to buckle, deform and ultimately fill the pore. In step 2, the deformation of vertical struts together with the applied load, initiate deformation in the form of elongation or shortening of the horizontal struts in the foam

structure. The aforementioned two steps of densification occur simultaneously and randomly, throughout the specimen. The process of densification continues until all the pores have been filled by the deformed struts. At the end of densification, the specimen essentially becomes a solid. Clearly, the densification phase constitutes the largest percentage of the total deformation of the metallic foam. Therefore, it is evident from figure 4 that, most of the energy absorption occurs in the densification phase.

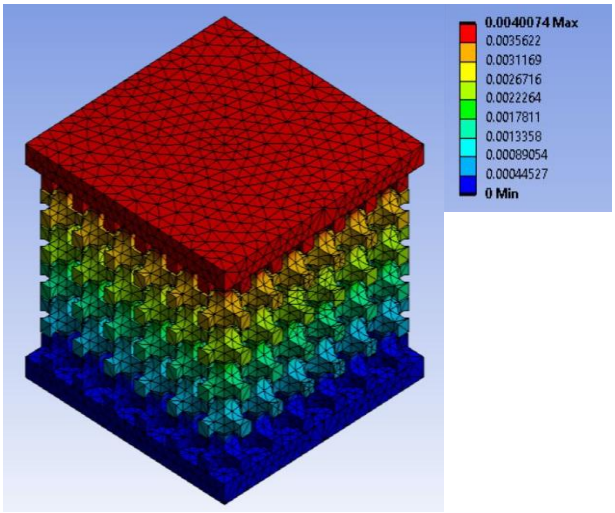

Figure 5. Simulated Force and Deformation.

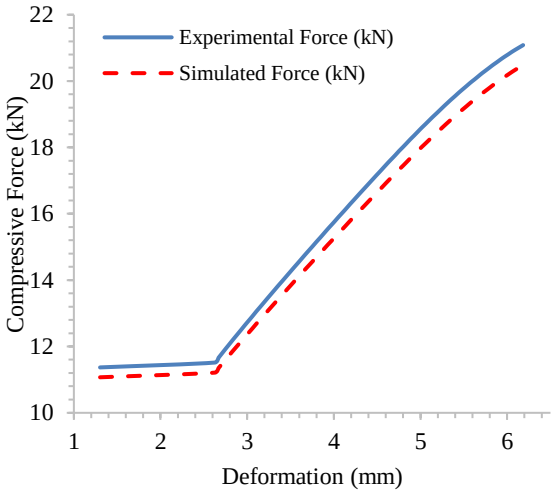

Figure 6. Estimation of Error.

In order to estimate the experimental results by computation, numerical models of the three specimens were analysed as detailed in section 2.4. The top surface of each specimen was subjected to compaction at incremental velocities of 1.3 mm/min, identical to the feed rate of the compression test. The built-in deformation and force probes in ANSYS Workbench were utilized to estimate the deformation and force experienced by the fixed support. These values were then compared with the experimental results and the numerical error was estimated. Figure 5 and figure 6 depict the aforementioned approach for specimen 1. This procedure was replicated for all the three specimens and it was observed that, the numerical simulation was validated by experimental results with the estimated error being less than 5 %.

4. Discussion

In line with established studies, it is evident from table 1 that, the foam porosities are inversely proportional to foam density [6]. The stress-strain graphs in figure 4 enable the estimation of the proof stress, defined as the stress at an offset of 0.2 % of the strain [7]. It can be observed from figure 4 that, for the specimen 3 with the pore size of 2 mm, the graph rises gradually and exhibits a uniform slope until a stress of 14 MPa. The corresponding proof stress was 1.3 MPa. It can also be deciphered from figure 4 that, the specimen 2 with a pore size of 2.5 mm shows a higher gradient until a stress of 20 MPa. This gradient is the highest of the three foams with the associated proof stress being 1.7 MPa. The gradient of specimen 1 with the pore size of 3 mm, extends to a stress of 18 MPa, with its stress-strain characteristics lying in between that of specimens 2 and 3. The proof stress in this case was 0.8 MPa. Additionally, complete densification of the specimen 3 is observed at a stress of 15 MPa.

A review of porosity, density and the stress-strain curves reveal that, specimen 2 having the lowest porosity and highest density exhibits the highest compressive strength of the three metal foams. The specimen 1 with the second highest density and second lowest porosity displays the second highest compressive strength. Specimen 3 exhibits the lowest compressive strength of all the three specimens considered. This analysis reveals that, compressive strength varies directly with density and inversely with porosity of the specimen. The aforesaid behaviour may be attributed to the enhanced resistance

offered by the interconnected struts of specimen 2 with pore size of 2.5 mm, in contrast to other specimens. Further, as pore size decreases to 2 mm, the foam effect decreases thereby, causing the specimen to behave similar to a solid. Since the simulation is validated, the numerical model can, in the future, be utilized to predict the behaviour of 3D printed metal foams for further improvements.

5. Conclusion

In the present study, metal foams of three porosities were modelled and 3D printed using a laser sintering process. The foams were subjected to compression and the stress-strain curves were plotted. Further, simulation studies were conducted on the metal foams and were compared with experimental results. The dimensional accuracy of the 3D printed porous metal foams was observed to be accurate. The study revealed that, the compressive behaviour was directly proportional to the densities and inversely proportional to the porosity of the metal foams. The simulation studies exhibited a proximate correlation with experimental results, signifying the validity of the numerical model.

References

[1] Wang X and Zhou G 2013*Rev. Adv. Mater. Sci.* **33**316-21
[2] Utsunomiya T, Hangai Y, Kubota N, Kuwazuru O and Yoshikawa N 2016*Mechanical Engineering Journal.***3**16-00149
[3] Bhogi S, Nampoothiri J, Ravi KR and Mukherjee M 2017 *Materials Science and Engineering.* A **685** 131-8
[4] Merabtine A, Gardan N, Gardan J, Badreddine H, Zhang C, Zhu F and Gong XL 2018 *The European Physical Journal Applied Physics*.**83**10904
[5] Novak N, Vesenjak M, Duarte I, Tanaka S, Hokamoto K, Krstulović-Opara L, Guo B, Chen P and Ren Z2019*Materials***12** 4108
[6] Ferfera RS and Madani B 2020 *International Journal of Heat and Mass Transfer.***148**119162
[7] Nakata T, Xu C, Ohashi H, Yoshida Y, Yoshida K and Kamado S 2020 *ScriptaMaterialia.* **180**16-22